Communication

Closed-cycle cold helium magic-angle spinning for sensitivity-enhanced multi-dimensional solid-state NMR

Yoh Matsuki [a], Shinji Nakamura [b], Shigeo Fukui [c], Hiroto Suematsu [b], Toshimichi Fujiwara [a,*]

[a] Institute for Protein Research, Osaka University, 3-2 Yamadaoka, Suita, Osaka 565-0871, Japan
[b] JEOL RESONANCE Inc., 3-1-2 Musashino, Akishima, Tokyo 196-8558, Japan
[c] Cryovac Corporation, 2-12-14 Chibune, Nishi Yodogawa, Osaka 555-0013, Japan

ABSTRACT

Magic-angle spinning (MAS) NMR is a powerful tool for studying molecular structure and dynamics, but suffers from its low sensitivity. Here, we developed a novel helium-cooling MAS NMR probe system adopting a closed-loop gas recirculation mechanism. In addition to the sensitivity gain due to low temperature, the present system has enabled highly stable MAS (v_R = 4–12 kHz) at cryogenic temperatures (T = 35–120 K) for over a week without consuming helium at a cost for electricity of 16 kW/h. High-resolution 1D and 2D data were recorded for a crystalline tri-peptide sample at T = 40 K and B_0 = 16.4 T, where an order of magnitude of sensitivity gain was demonstrated versus room temperature measurement. The low-cost and long-term stable MAS strongly promotes broader application of the brute-force sensitivity-enhanced multi-dimensional MAS NMR, as well as dynamic nuclear polarization (DNP)-enhanced NMR in a temperature range lower than 100 K.

© 2015 The Authors. Published by Elsevier Inc. This is an open access article under the CC BY license (http://creativecommons.org/licenses/by/4.0/).

1. Introduction

Solid-state magic angle spinning NMR (MAS NMR) is one of the most powerful tools to study structure and dynamics of amorphous molecular systems including polymers [1], inorganic materials [2] and bio-macromolecules [3], but suffers from its low sensitivity. Sensitivity enhancement of MAS NMR is possible with a variety of approaches including the use of the cross-polarization (CP), high field magnets, cold sample and/or RF circuitry [4,5], non-uniform sampling [6], accelerated longitudinal relaxation [7], and a variety of hyper-polarization methods such as the dynamic nuclear polarization (DNP) [8]. Among them, one of the conceptually simplest and the most general approaches would be to use high static field (B_0) and low temperature. Lowering sample temperature (T) linearly increases the Boltzmann nuclear polarization within the Curie regime, and lowering the circuit temperature reduces the thermal noise. In combination, the sensitivity enhancement by a factor of up to ~40 is anticipated at T = 25 K (and a similar temperature for the RF circuitry) [9], and the effect has been observed indeed in experiments with static [9] and MAS conditions [10,11]. As to the sensitivity gain with increasing B_0, it is often referred to as being

proportional to $B_0^{3/2}$. Importantly and quite uniquely, these sensitivity gains are realized for any spin species (e⁻, ¹H, ¹³C etc) with any spin quantum number (I = 1/2 or >1/2), and irrespective of molecular structure or sample composition.

In addition to the sensitivity gain, low temperature MAS NMR allows for studying phenomena accessible only at low temperatures, ranging from the Hall effect in two dimensionally confined electrons [12], super conduction [13] to cryo-trapping of protein intermediates [14] and ultra low energy-barrier molecular/molecular segmental motion [15,16]. The DNP-enhanced NMR spectroscopy represents yet another important application of the cryogenic MAS capability because the reduced spin relaxation at low temperatures improves the efficiency of DNP, compensating for its relative inefficiency at high-field i.e. high-resolution conditions [17,18].

Although promising, cryogenic MAS NMR at $T \ll 90$ K that is possible with cold helium for cooling and/or spinning the sample has not been widely used in recent applications of MAS NMR. The unpopularity emanates from a number of technical difficulties: (1) Low kinematic viscosity of cold helium gas tends to hamper stable MAS [19,20]. (2) Long-term operation such as for a week often required for biological samples is difficult since the pressurized helium boiler dewar used in conventional setups is difficult to refill during experiments [11,17,20]. (3) Helium is expensive and the running cost tends to be too high for a routine use. In a design of Tycko et al. [10], cold helium gas was used only for the sample

---

* Corresponding author.
  E-mail address: tfjwr@protein.osaka-u.ac.jp (T. Fujiwara).

temperature control, while nitrogen gas for the sample spinning. Although this approach reduces the helium consumption, it contaminates helium with nitrogen, making the recycling of the spent helium gas more challenging. (4) The probe can be arcing-prone under helium atmosphere that introduces severe noises in NMR data. (5) Signal broadening either due to the frozen conformational disorder or the interference effect between slowed molecular motion and the decoupling field/MAS can degrade the spectral resolution.

Here, we developed a novel *closed-cycle* helium-cooling MAS NMR probe system operating at $B_0 = 16.4$ T (700 MHz for ^{1}H frequency), with the primary interest being on the low temperature enhancement of the sensitivity, but also on an engineering challenge for alleviating general issues associated with the cryogenic MAS with a view to using it in DNP NMR experiments. With our new system indeed, the above-mentioned difficulties (1)–(4) are resolved, and the (5) is significantly mitigated as is demonstrated below.

2. Instruments

Fig. 1 overviews our closed-cycle helium-cooling MAS NMR probe system. The system consists of a Cryogenic Helium Circulation (CHC) unit (Fig. 1a and d) and a compatible 16.4 T DNP MAS NMR probe system (Fig. 1b and c). The CHC unit is on casters, and can be shared among spectrometers equipped with the compatible NMR probe, and its installation requires only small area near the NMR magnet (Fig. S1).

2.1. Cryogenic Helium Circulation (CHC) unit

The CHC unit (Fig. 1a and d) consists of a heat exchanger box, and a rack for compressors, buffer tanks and mass flow controllers (MFCs). The vacuum insulated heat exchanger box encases two 10-Kelvin GM coolers (Sumitomo Heavy Industries, Ltd., SRDK-408S-A71A), one each on the bearing and driving gas line. Helium gas is introduced to the CHC unit from a gas cylinder
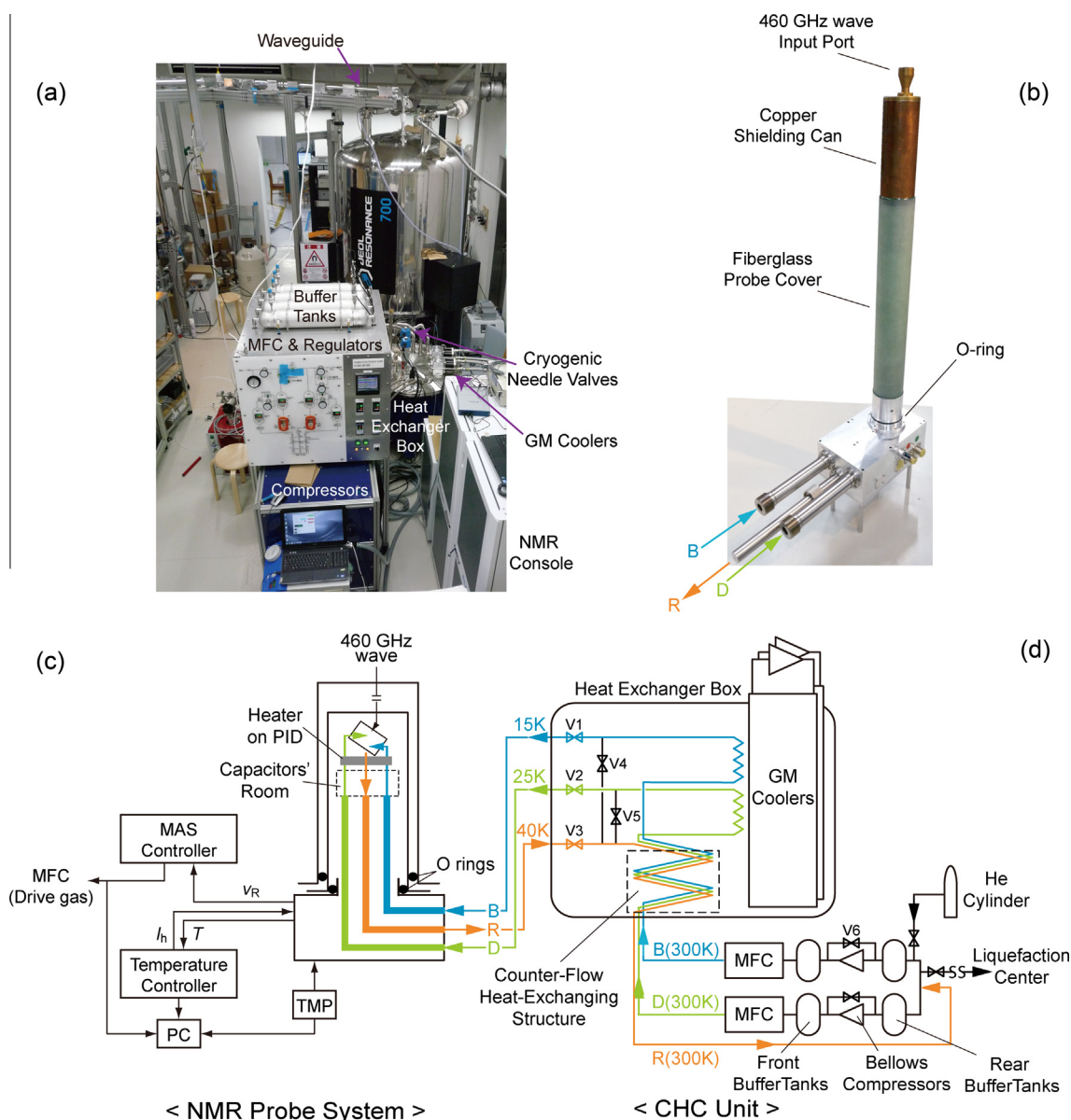

Fig. 1. Photographs of (a) the CHC unit together with the 16.4 T NMR spectrometer, and (b) the compatible DNP-NMR probe. (c and d) A schematic diagram of the system. The gas streams labeled with "B", "D" and "R" stand for the bearing, driving and return gases. v_R, I_h and T represents the MAS rate, the heater current, and the sample temperature, respectively.

outside the room using a dedicated stainless steel gas line, and after use can be vented to liquefaction center on campus (∼500 m away from the NMR room).

The bellows compressor (IBS Inc., MB-602) can produce ∼100 L/min of pressurized (typically <0.25 MPa in the front buffer tanks) gas flow on each of the driving and bearing gas line. The buffered spinner gases are further regulated with precision MFCs (HORIBA/STEC Inc., SEC-N132MGM), then sent to the heat exchanger box. The heat exchanger is able to cool ∼150 L/min of helium gas from room temperature to ∼20 K on a 15 kW power input. The cold gas thus produced is transferred to the NMR probe using vacuum-jacketed flexible transfer tubes. The gas returned from the NMR probe being still very cold (∼40 K) is used in the initial gas cooling stage using a tube-in-tube type counter-flow heat exchanging system (Cryovac Corp.) [21]. This latter step warms the return gas to ambient temperature, fully exploiting the cooling capacity of the cold gas. Resultant warm gas is filtered, and split into the rear buffer tanks before re-entering the original bellows compressors, completing a closed loop. The pathway for the spinner gases throughout is made hermetic to avoid contamination of helium with atmospheric nitrogen and moisture. Bellows compressor does not use oil lubrication, and free from contamination of the spinner gases. The filters, compressors, buffer tanks and MFCs are all operated at room temperature, and required no cryogenic specifications.

2.2. 16.4 T DNP NMR probe

The CHC-compatible DNP NMR probe system (Fig. 1b and c) consists of an NMR probe, a temperature controller (Lake Shore Cryotronics, Inc, Model 335), an MAS controller (JEOL RESONANCE Inc.), a turbo molecular pump (TMP) (Osaka Vacuum, Ltd., TG350F), and a LabVIEW PC. The LabVIEW console continuously logs on the spinner gas flow, MAS rate, sample temperature, and the probe vacuum. The probe's cylindrical body is covered with a jacket (OD = 70 mm), and the space in-between is pumped with the TMP for heat insulation. The probe together with the jacket is inserted to a standard room-temperature shim stack installed in the 89 mm-magnet bore. Since the probe weighs only ∼5.5 kg, one can easily lift it.

In the probe, three vacuum-jacketed lines provide paths for delivering/returning the spinner gases to/from the MAS module in the sample room at the probe top: two lines deliver the driving and bearing gases independently, and another one for returning the spent helium to the outlet port. The temperature of the spinner gases is regulated just before the entry to the MAS module using a 50 W heater block on a feedback regulation. The helium gas discharged from the MAS module is routed through a capacitors' room located just below the sample room, where it cools the tuning/matching capacitors (Fig. 1c), then collected to a return gas line. In this configuration, the RF coil, the leads and the capacitors are all located in a cold helium atmosphere under a slightly positive pressure on gauge.

The RF coil is a 10 mm-long 3-turn solenoid wound from a 1 mm-diameter silver-plated copper wire, covering the 5 mm-long active sample space of a 3.2-mm phi rotor. The wire spacing was made relatively large (∼2 mm) to facilitate the microwave irradiation of the sample. Microwave is introduced from the probe top, and irradiates the sample transversely across the RF coil.

3. Results and discussion

3.1. Cryogenic MAS

Before an operation, the system needed to be thoroughly purged with high purity helium gas (99.999%), and the vacuum sections in the probe to be pumped to 10^{-3} Pa or better. In the initial stage of the sample cooling, it was important to keep the MAS rate low (∼2 kHz) until the sample temperature reaches ∼100 K considering insufficient bearing gas flow, i.e. insufficient bearing stiffness at high temperatures. The MAS rate was then gradually increased to the target rate, and the probe heater is turned on with a target temperature set on the controller. It typically takes ∼6 h overall to cool the sample from room temperature to $T = 35$ K, but significantly faster if the heat-exchanger box is pre-cooled (see below). Typical amount of helium required for the operation was ∼0.7 L (liq.) including the gas for the purging and for maintaining the cryogenic MAS. Only one GM cooler on the bearing line sufficed to achieve the higher temperature range ($T = 120–70$ K), while both were required for the lower range ($T = 70–35$ K).

To change samples, the probe was disconnected to warm up (takes ∼1 h), while the cold gas was kept circulated in the CHC unit by closing the valves V1–3, and opening V4–5 (Fig. 1d). Since the CHC unit that represents the majority of the heat capacity of the system is preserved cold, the probe re-cooling process goes very quickly, and takes only an hour to reach $T \sim 40$ K again. Thus, overall, sample can be exchanged in a two-hour process. Taking advantage of the ability to cool the CHC unit independently to the NMR probe, the startup procedure can be streamlined by cooling only the CHC unit unattended overnight, and start cooling the sample in the morning.

We used a standard MAS module for "3.2 mm rotors" (JEOL RESONANCE Inc.), whereas carefully optimized the rotor diameter for stable MAS at $T = 35$ K. The active sample volume is ∼25 μL, being suitable to studies on bulky biological samples such as membrane proteins and proteins in-cell. The maximum MAS frequency with the present setup was $v_R = 4$ kHz at $T = 35$ K while generally faster MAS was achievable at higher temperatures, for instance 4.7 kHz at 40 K, 6.4 kHz at 60 K, and 9.5 kHz at 95 K. The maximum MAS rate is currently limited by insufficient driving gas flow; an additional bellows compressor on the driving gas line is currently under test. A smaller rotor would suffice for studies on small molecules, and should allow for faster MAS [11]. Lower sample temperature should also be achievable with additional GM cooler(s), and/or improved probe insulation.

One of the most compelling advantages of the present *in-situ* gas recirculation system is its excellent long-term stability. Fig. S2 demonstrates stable MAS ($v_R = 4$ kHz) and temperature ($T = 40$ K) for over 2.5 days, during which the standard deviation fluctuation for the MAS rate and temperature was ±5 Hz and ±0.5 K, respectively. Similar stability was observed at all temperatures and MAS rates tested. So far, more than 14 days of continuous and stable run has been confirmed, during which no gas pressure/flow drop was observed, thus even longer run seems to be possible.

The MAS rate was very stable without any feedback regulation since the gas flow was inherently very stable; we are not boiling off or heat exchanging to liquid cryogen for the production of the cold spinner gases. Only a small (±15 Hz) and slow oscillation (time period on the order of a day) was observed for the MAS rate, presumably due to the change in the cooling capacity of the GM coolers that weakly depends on the environment temperature, but this was removed by setting the maximum driving gas flow at the MFC. The sample temperature was also very stable and reproducible, which is crucial for temperature-specific experiments e.g. on the molecular dynamics and the spin relaxation.

Low running cost is another major advantage of the closed-cycle gas circulation system. The running cost was almost exclusively for the electricity expense for the GM coolers, and was only ∼$3/h based on our local electricity price of ∼¢18/kW h. This corresponded to ∼1/30th of our previous design, where liquid helium was boiled for the production of cold spinner gases [17].

3.2. NMR experiments

The RF circuit is doubly tunable to frequencies 700 ± 20 MHz and 175 ± 20 MHz, covering the ^{1}H and ^{13}C Lamor frequencies, respectively, at $B_0 = 16.4$ T. The three-turn solenoid coil with wide spacing facilitated the microwave irradiation, while did not decrease its RF efficiency critically. The nutation frequency of 100 kHz was obtained for ^{1}H with the probe-in power of 30 W, and 40 kHz for ^{13}C with 120 W at $T = 40$ K. Very similar efficiency was found at $T = 95$ K. The B_1 inhomogeneity was measured to be $\pm 5.5\%$ for both ^{1}H and ^{13}C fields. The geometry of the RF coil can be improved for a better B_1 homogeneity and the microwave transmission efficiency.

The probe is compatible with a standard room-temperature shim stack, allowing for the regular high-resolution MAS NMR. After a brief manual shimming, the linewidth of 0.09 ppm (full width at half height, FWHH) was obtained for the methine ^{13}C signal of adamantane (not shown). Fig. 2 shows a 1D {^{1}H}–^{13}C CP spectrum of uniformly ^{13}C, ^{15}N-labeled crystalline tri-peptide *N-formyl*-Met-Leu-Phe-OH (MLF), recorded with the MAS rate of 4.7 kHz at $T = 300$ K and 40 K. At 300 K, typical line width (FWHH) for the carbonyl, C^α and methyl carbon signals was 0.75, 1.05 and 0.50 ppm, respectively. With faster MAS, even sharper lines were observed with better removal of the residual dipolar broadening (Fig. S3).

On the NMR side, the primary benefit from the use of cryogenic MAS is the sensitivity gain from the Boltzmann factor and the reduced thermal noise. The ratio of the integral spectral intensity measured for the aliphatic region (10–60 ppm) of the CP spectra taken at 40 K (Fig. 1b) to the one at 300 K (Fig. 1a) was ~7.1, being close to the inverse of the temperature ratio, $1/(40/300) = 7.5$. The comparison was made at the cross-polarization time that maximizes the signal intensity at respective temperature, and with the recycle delay much longer than the longitudinal relaxation ($\gg 5 * T_{1H}$, where T_{1H} was 1.2 s and 5.6 s at 300 K and 40 K, respectively). A similar ratio of 7.2 was obtained in a comparison of the single-pulse excitation ^{13}C spectra taken at 300 K and 40 K with a long enough recycle delay ($\sim 5 * T_{1C}$, where T_{1C} is the longitudinal relaxation time of ^{13}C, and was 1 s and 400 s at 300 K and 40 K, respectively). The RMS noise level measured at 40 K was found to be 1.3 times smaller than that at 300 K due to the cold sample, RF coil, leads and the capacitors. Cooling preamps and duplexer altogether [4,5] should reduce the thermal noise level further. The overall sensitivity we gained from the cryogenic MAS experiment was thus larger by a factor of ~9 ($=7 * 1.3$) versus room temperature measurements. On top of this, the sensitivity should also be scaled in proportion to $\sim B_0^{3/2}$, which is roughly verified in experiments using our well-standardized spectrometers operating at 500, 600 and 700 MHz (Fig. S4). Thus, a factor of 2.3 additional gain may be stated for the measurements at $B_0 = 16.4$ T versus, for example, measurements with more ubiquitous magnet operating at $B_0 = 9.4$ T, ending up with an overall gain exceeding a factor of 20.

At even lower temperatures, more sensitivity gain should result. In our current setup, the major heat load was the NMR probe, for which the heat insulation has not been fully optimized yet. A simple modification such as the installation of BoPET super-insulation layers on the probe body is expected to improve the lowest achievable temperature by 10 K or more. Excessively long spin relaxation possible at ultra low temperatures could be alleviated by the use of relaxation agent [7,22]. For DNP measurements, addition of some paramagnetic dopants is required anyway.

At 40 K (Fig. 2b and c), the linewidth for the carbonyl and C^α signals increased only by less than 15%, suggesting only minor distribution of the backbone conformers. On the other hand, significant change in the signal intensity/linewidth was observed for the side chain aromatic and methyl carbons. This is attributed to the
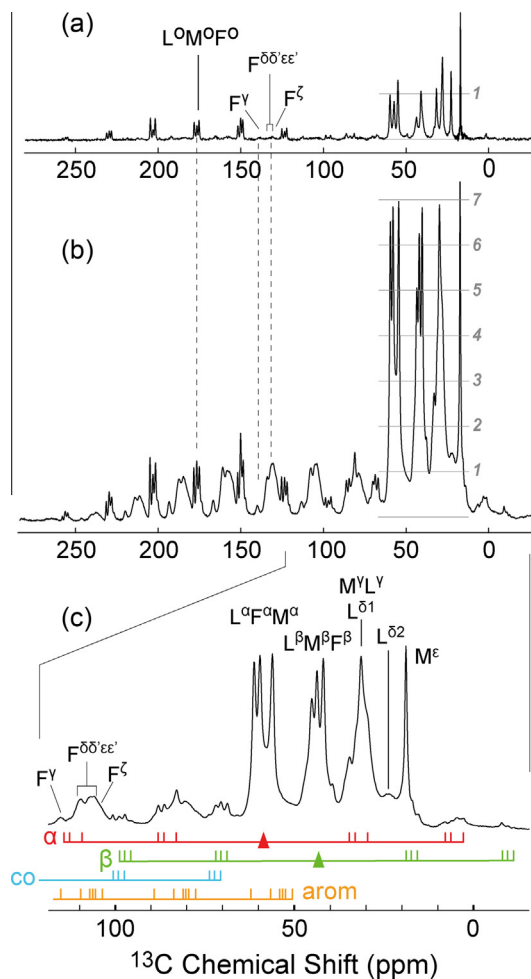

Fig. 2. {^{1}H}–^{13}C CP spectrum of MLF taken (a) at $T = 300$ K with 4 scans, and (b) at 40 K, 8 scans. The MAS rate was 4.7 kHz. The spectrum in (b) is vertically scaled for equivalent unit-time noise amplitude to that in (a). (c) Aliphatic region of the spectrum in (b). Positions of the SSBs are indicated below the spectrum. The CP period was 1.0 ms and 0.25 ms at 300 K and 40 K, respectively, and the RF fields were 45 kHz and 35 kHz for ^{1}H and ^{13}C, respectively. High-power ^{1}H decoupling (70 kHz) was applied during the 10 ms-data acquisition. About 7 mg of MLF crystal was packed together with powder of KBr so that the magic angle and the sample temperature could be checked in situ. The data were taken with a JEOL ECA 700II spectrometer. No window function was applied.

slow-down of the peptide side chain dynamics and its interference with the decoupling RF field, which has been observed also at higher temperatures (~100 K) [15,23]. For instance at 40 K, all four aromatic C^δ and C^ϵ carbons of phenylalanine (Phe) side chain at δ ($C^{\delta/\epsilon}$) ~132 ppm show partly overlapped signals with seemingly comparable linewidth and intensity to other aromatic signals (Fig 2b), indicating that the ring flipping is in the slow exchange regime. At room temperature (Fig. S3), the same set of signals is strongly broadened [23]. A similar interference broadening was observed also for methyl signals, but at cryogenic temperature regime (Fig. 2c), reflecting the much lower energy barriers for the methyl group rotation than the phenyl ring flipping. Remarkably, one of the two methyl ($C^{\delta2}$) signals of leucine (Leu) at $\delta(C^{\delta2}) \sim 23$ ppm was broadened by a factor of 10 or more at 40 K with respect to the room-temperature spectrum (Fig. 2b and c), and it was difficult to reliably measure the linewidth from the 1D data. Virtually identical broadening was observed also in the ^{13}C direct excitation spectrum (Fig. S5).

It is interesting to see that the Leu $C^{\delta2}$ signal was broadest at $T \sim 90$ K, and became slightly sharper again at $T = 40$ K (Fig. S6), suggesting the maximum interference occurring at 90 K range. In
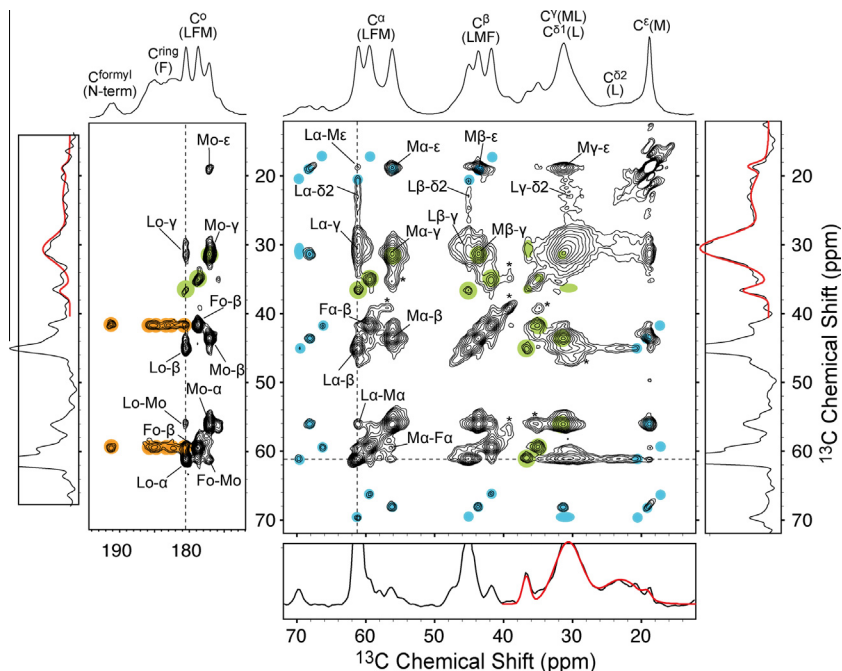
Fig. 3. Two-dimensional PDSD spectrum of MLF recorded at $\nu_R = 4.3$ kHz and $T = 40$ K using 1 ms for the CP period, 25 ms for the mixing, and 7 ms for the data acquisition. For each t_1 sampling point, two transients were acquired, and total 330 complex t_1 points were collected for the maximum t_1 evolution of 7 ms. High power ^{1}H decoupling (70 kHz) was used for the evolution and detection periods. The experiment was setup in a way that a dummy decoupling period follows the data acquisition period so that it compensates for the changing length of the t_1 evolution period, thus all t_1 samples experience identical power load. Total acquisition time was 10 h with the recycle delay of 30 s (>5 * T_{1H}). The MAS frequency was chosen so that any SSBs are not on top of the Leu $C^{\delta2}$ methyl signal. The cross peaks to SSBs of C^α, C^β and aromatic carbons are highlighted in green, blue and orange, respectively. Asterisks indicate some minor unassigned peaks. One-dimensional slices are taken at the dotted lines, and shown with the results of Gaussian fittings for the high field region (10–40 ppm) in red. (For interpretation of the references to color in this figure legend, the reader is referred to the web version of this article.)

contrast, the Met C^ε methyl signal at $\delta(C^\varepsilon) \sim 19$ ppm exhibited progressive broadening in the same temperature range: FWHH was 0.45 ppm, 0.7 ppm and 0.9 ppm at 300 K, 90 K and 40 K, respectively. This suggests a much less rotation hindrance for the Met C^ε methyl group than for Leu $C^{\delta2}$. This latter broadening of Met C^ε signal due to ultra-low energy barrier rotation was not mentioned in the previous work at higher temperature ($\sim$100 K) [15]. The variability of the methyl signal linewidth over amino-acid residues in a peptide/protein or even for two methyl groups in a side chain suggests an interesting possibility of quantifying the local steric environment by simply measuring linewidth, and of interpreting it in terms of the protein packing or protein–protein interaction. A study in this direction is underway.

The rotation of methyl groups still seems to provide a viable relaxation process for protons: the ^{1}H T_1 was 5.6 s at $T = 40$ K without paramagnetic doping. Thus, for compounds containing methyl groups in high density, being often the case for peptide/protein assemblies, such as membrane-embedded proteins and protein fibrils, the recycle delay seems not to be a limiting issue for signal averaging and multi-dimensional measurements at the present temperature range.

The excellent long-term stability of the system greatly facilitated data acquisition in high dimensions at cryogenic temperatures. As mentioned above, it is often difficult to fully characterize the broad spectral features only in 1D spectra, such as the strongly broadened Leu methyl $C^{\delta2}$ signal, due to the spectral overlap. In 2D or higher dimensions, we gain a lot more opportunities in resolving those broad lines. Fig. 3 shows an example of a 2D ^{1}H-driven spin diffusion (PDSD) spectrum of MLF recorded at $T = 40$ K. The temperature and MAS frequency were stable well over the 10-h data acquisition for each 2D data. The stability of MAS can be verified by the sharp cross-peaks to the SSBs as highlighted with color in Fig. 3. What is also remarkable is that we have

experienced absolutely no probe arcing during the measurement even under the total 15 ms-long high power ^{1}H irradiation under helium atmosphere. The absence of the probe arcing can be attributed to the relatively high helium flow (>150 L/min) and the slightly positive pressure on gauge (i.e., >0.1 MPa) around the RF circuitry, which significantly reduces the mean free path of the field-ionized helium gas.

Due to the increased spectral resolution in the 2D spectrum, the linewidth of the strongly broadened Leu $C^{\delta2}$ methyl signal could be readily measured. Since some of the cross peaks to Leu $C^{\delta2}$ signal, such as the intra-residue C^α–$C^{\delta2}$ cross peak (labeled with "Lα-δ2" in Fig. 3), were clearly resolved, the 1D slice was reliably fitted to measure the linewidth of 1150 ± 50 Hz, i.e. $\sim$6.6 ppm. We note that this exemplifies the quantification of extremely broad line considering the fact that the typical line broadening due to the frozen distribution of peptide/protein conformers would be up to $\sim$4 ppm. Thus, the long-term stability of the cryogenic MAS provides an excellent basis for characterizing in high dimension broad spectral features often encountered in low temperature spectra.

4. Conclusions

We have designed, built and tested a novel *closed-cycle* helium-cooling and -spinning NMR probe system. To our knowledge, this is the first experimental demonstration of an *in-situ* gas recirculation system for cryogenic MAS NMR.

The present system was able to maintain highly stable MAS ($\nu_R = 4$–12 kHz) at cryogenic temperatures ($T = 35$–120 K) without consuming helium. The stability of temperature (±0.5 K) and the MAS frequency (±5 Hz) was also excellent for an extended period of time, such as weeks, with the running cost as low as $\sim$\$3/h. In addition, the probe is compatible with a standard room

temperature shim stack, and allows for the full high-resolution MAS NMR spectroscopy, which was illustrated with 1D and 2D data recorded for a uniformly labeled microcrystalline tri-peptide (MLF). In the 2D data, the linewidth of a methyl signal with a severe interference broadening was measured (FWHH = 1150 Hz or 6.6 ppm), illustrating the improved resolving power for broad spectral features often encountered at low temperatures. Recording even higher dimensional data at T = 40 K seems to be straightforward.

An order of magnitude sensitivity gain we observed at T = 40 K is a result of the linear increase of the Boltzmann polarization and the decrease of the thermal noise due to the cold sample and the RF components. Another order of magnitude increase of sensitivity is expected from DNP. The probe is equipped with a 460 GHz micro-wave irradiation structure, and thus our system enables DNP-enhanced spectroscopy in the temperature range between 35 K and 120 K. Overall, the present system has resolved some of the major limitations associated with the cryogenic MAS with conventional setups, and will significantly expands the scope of the brute-force sensitivity enhanced multi-dimensional MAS NMR, as well as the high-field DNP. The simple and easy operation of the system also greatly adds to users' benefits, and will appeal to a wide range of chemists, biochemists and material scientists.

Acknowledgments

Appendix A. Supplementary data

Supplementary data associated with this article can be found, in the online version, at http://dx.doi.org/10.1016/j.jmr.2015.08.003.

References

[1] M.R. Hansen, R. Graf, H.W. Spiess, Solid-state NMR in macromolecular systems: insights on how molecular entities move, Acc. Chem. Res. 46 (2013) 1996–2007.

[2] S.H. Li, F. Deng, Recent advances of solid-state NMR studies on zeolites, Annu. Rep. NMR Spectro. 78 (2013) 1–54.

[3] S. Yan, C.L. Suiter, G.J. Hou, H.L. Zhang, T. Polenova, Probing structure and dynamics of protein assemblies by magic angle spinning NMR spectroscopy, Acc. Chem. Res. 46 (2013) 2047–2058.

[4] P. Styles, N.F. Soffe, C.A. Scott, D.A. Cragg, F. Row, D.J. White, P.C.J. White, A high-resolution NMR probe in which the coil and preamplifier are cooled with liquid-helium, J. Magn. Reson. 60 (1984) 397–404.

[5] T. Mizuno, K. Takegoshi, Development of a cryogenic duplexer for solid-state nuclear magnetic resonance, Rev. Sci. Instrum. 80 (2009) 124702.

[6] Y. Matsuki, M.T. Eddy, R.G. Griffin, J. Herzfeld, Rapid three-dimensional MAS NMR spectroscopy at critical sensitivity, Angew. Chem. Int. Ed. 49 (2010) 9215–9218.

[7] N.P. Wickramasinghe, S. Parthasarathy, C.R. Jones, C. Bhardwaj, F. Long, M. Kotecha, S. Mehboob, L.W.M. Fung, J. Past, A. Samoson, Y. Ishii, Nanomole-scale protein solid-state NMR by breaking intrinsic [1]H T_1 boundaries, Nat. Methods 6 (2009) 215–218.

[8] L.R. Becerra, G.J. Gerfen, R.J. Temkin, D.J. Singel, R.G. Griffin, Dynamic nuclear-polarization with a cyclotron-resonance maser at 5T, Phys. Rev. Lett. 71 (1993) 3561–3564.

[9] A.S. Lipton, J.A. Sears, P.D. Ellis, A general strategy for the NMR observation of half-integer quadrupolar nuclei in dilute environments, J. Magn. Reson. 151 (2001) 48–59.

[10] R. Tycko, NMR at low and ultra low temperatures, Acc. Chem. Res. 46 (2013) 1923–1932.

[11] M. Concistre, O.G. Johannessen, E. Carignani, M. Geppi, M.H. Levitt, Magic-angle spinning NMR of cold samples, Acc. Chem. Res. 46 (2013) 1914–1922.

[12] R. Tycko, S.E. Barrett, G. Dabbagh, L.N. Pfeiffer, K.W. West, Electronic states in gallium-arsenide quantum-wells probed by optically pumped NMR, Science 268 (1995) 1460–1463.

[13] P. Beckett, M.S. Denning, I. Heinmaa, M.C. Dimri, E.A. Young, R. Stern, M. Carravetta, High resolution ^{11}B NMR of magnesium diboride using cryogenic magic angle spinning, J. Chem. Phys. 137 (2012) 114201.

[14] V.S. Bajaj, M.L. Mak-Jurkauskas, M. Belenky, J. Herzfeld, R.G. Griffin, Functional and shunt states of bacteriorhodopsin resolved by 250 GHz dynamic nuclear polarization-enhanced solid-state NMR, Proc. Natl. Acad. Sci. U.S.A. 106 (2009) 9244–9249.

[15] V.S. Bajaj, P.C.A. van der Wel, R.G. Griffin, Observation of a low-temperature, dynamically driven structural transition in a polypeptide by solid-state NMR spectroscopy, J. Am. Chem. Soc. 131 (2009) 118–128.

[16] C. Beduz, M. Carravetta, J.Y.C. Chen, M. Concistre, M. Denning, M. Frunzi, A.J. Horsewill, O.G. Johannessen, R. Lawler, X.G. Lei, M.H. Levitt, Y.J. Li, S. Mamone, Y. Murata, U. Nagel, T. Nishida, J. Ollivier, S. Rols, T. Room, R. Sarkar, N.J. Turro, Y.F. Yang, Quantum rotation of ortho and para-water encapsulated in a fullerene cage, Proc. Natl. Acad. Sci. U.S.A. 109 (2012) 12894–12898.

[17] Y. Matsuki, K. Ueda, T. Idehara, R. Ikeda, I. Ogawa, S. Nakamura, M. Toda, T. Anai, T. Fujiwara, Helium-cooling and -spinning dynamic nuclear polarization for sensitivity-enhanced solid-state NMR at 14 T and 30 K, J. Magn. Reson. 225 (2012) 1–9.

[18] E.J. Koers, E.A.W. van der Cruijsen, M. Rosay, M. Weingarth, A. Prokofyev, C. Sauvee, O. Ouari, J. van der Zwan, O. Pongs, P. Tordo, W.E. Maas, M. Baldus, NMR-based structural biology enhanced by dynamic nuclear polarization at high magnetic field, J. Biomol. NMR 60 (2014) 157–168.

[19] F.D. Doty, P.D. Ellis, Design of high-speed cylindrical NMR sample spinners, Rev. Sci. Instrum. 52 (1981) 1868–1875.

[20] V. Macho, R. Kendrick, C.S. Yannoni, Cross polarization magic-angle spinning NMR at cryogenic temperatures, J. Magn. Reson. 52 (1983) 450–456.

[21] T. Mito, N. Yanagi, Y. Ogawa, J. Morikawa, K. Ohkuni, M. Iwakuma, T. Uede, S. Nose, I. Itho, S. Fukui, T. Nagayama, J. Okuno, Design and construction of a Mini-RT device, J. Cryogenics Supercond. Soc. Jpn. 39 (2004) 182–192.

[22] K.R. Thurber, R. Tycko, Biomolecular solid state NMR with magic-angle spinning at 25 K, J. Magn. Reson. 195 (2008) 179–186.

[23] A.B. Barnes, B. Corzilius, M.L. Mak-Jurkauskas, L.B. Andreas, V.S. Bajaj, Y. Matsuki, M.L. Belenky, J. Lutgenburg, J.R. Sirigiri, R.J. Temkin, J. Herzfeld, R.G. Griffin, Resolution and polarization distribution in cryogenic DNP/MAS experiments, Phys. Chem. Chem. Phys. 12 (2010) 5861–5867.